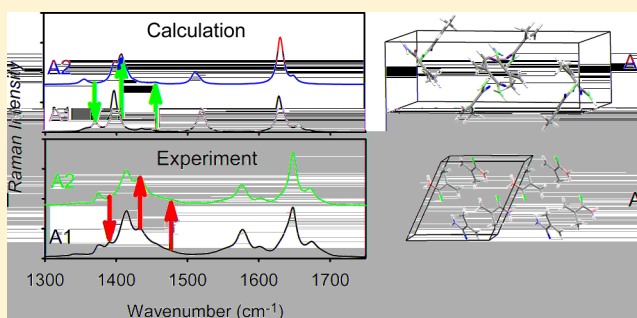


Resolution of Organic Polymorphic Crystals by Raman Spectroscopy

Martin Dračinský,^{†,‡} Eliška Procházková,[†] Jiří Kessler,[†] Jaroslav Šebestík,[†] Pavel Matějka,[§] and Petr Bour^{*,†}[†]Institute of Organic Chemistry and Biochemistry, Academy of Sciences, Flemingovo nám. 2, 166 10 Prague, Czech Republic[‡]Department of Chemistry, Durham University, South Road, Durham DH1 3LE, United Kingdom[§]Department of Physical Chemistry, Institute of Chemical Technology, Technická 5, 166 28 Prague, Czech Republic

Supporting Information

ABSTRACT: Depending on crystallization conditions, many organic compounds can form crystals of different structure. Their proper characterization is important, for example, in the pharmaceutical industry. While the X-ray diffractometry established as a standard method, alternative techniques are desirable for broader application flexibility and economic reasons. In the present study, Raman spectroscopy combined with the density functional calculations is suggested as a complementary method to the X-ray and other higher resolution techniques. The potential to discriminate structural differences in polymorphic crystalline forms is documented on three model compounds of industrial importance. Methacrylamide, piracetam, and 2-thiobarbituric acid were crystallized under various conditions, and their Raman spectra were recorded using 532 and 1064 nm laser excitations. X-ray diffractometry and nuclear magnetic resonance spectroscopy were used as complementary techniques to verify sample composition and structure. To interpret the observed differences in Raman frequencies and intensities, three computational strategies were explored based on single molecule, a cluster model, and a plane-wave periodic boundary conditions calculation. The single-molecule modeling was found inadequate, whereas the plane-wave approach provides the most realistic spectra. For all compounds, the differences in the Raman spectra of polymorphic forms could be unambiguously assigned to the simulations. The modeling revealed that the spectral differences were caused by the molecular structure itself as well as by crystal packing. The relative importance of these factors significantly varied across the investigated samples. Owing to its simplicity, Raman spectroscopy appears to be a promising technique capable of reliable discriminating between organic crystal polymorphic states.



INTRODUCTION

Many elements, ionic compounds, or molecules can form crystals of more than one structure. This behavior, polymorphism, is also encountered in single-component organic crystals.¹ Individual crystal forms can then exhibit different physical or even chemical properties.² The identification of polymorphic forms is therefore of crucial importance, for example, in the pharmaceutical industry. Various pharmaceutical processes yield different polymorphs, hydrates, and solvates of drugs.^{3–5} In particular, the crystalline state of a given compound influences its bioavailability, or just the production cost, as it may be easier to make drugs from one polymorph than from another. Drug regulatory authorities such as FDA in USA demand information about polymorphism before granting licenses for product distribution. Even patents have been made on the basis of the discovery of new polymorphs.^{6–8}

Apart from polymorphs that have the same molecular composition, organic substances can form various solvates or hydrates, which is sometimes referred to as pseudopolymorphism.⁹ Inclusion of more than one molecule in the asymmetric part of the unit cell ($Z' > 1$) represents yet another

interesting crystal variation.^{10,11} Complementary to the standard diffraction methods, the ¹³C cross-polarization (CP) magic-angle spinning (MAS) NMR is also an efficient way of determining Z' by means of comparing the number of observed resonances with the number of nonequivalent carbon atoms present in the molecule.^{5,12} Polymorphic crystals were also successfully studied by neutron diffraction.¹³

In the present study, we explore the potential of Raman spectroscopy to reliably distinguish three model polymorphic crystals. The low-resolution spectroscopic methods are often more practical than the X-ray diffraction or NMR, e.g., samples are easier to prepare and/or a smaller amount is required, and the spectra can be collected faster. Raman scattering is very sensitive to fine structural details in crystals and is thus increasingly used in analytical chemistry.^{14–19} It measures the relative intensity of scattered light as dependent on its shift from the laser excitation frequency, usually caused by

Received: May 3, 2013

Revised: May 25, 2013

Published: May 30, 2013

vibrational motions in molecules. In terms of sample preparation, the Raman technique resembles X-ray powder diffraction, where polycrystalline samples are used as well.

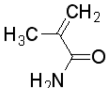
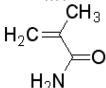
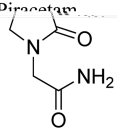
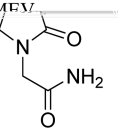
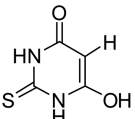
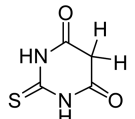
Lately, the vibrational Raman spectroscopy in the solid state has been boosted by the possibility to reliably simulate spectra of infinite periodic systems by accurate quantum-chemical methods. In particular, the plane-wave density functional theory (DFT) methodology is convenient as it allows for the crystalline translational symmetry.²⁰ However, we are not aware of any systematic accuracy test with respect to the discrimination of the polymorphic crystal vibrational spectra. Especially for organic molecules bound by weak crystal forces, high-precision computations are required to detect the finer crystal structure differences.

To assess the potential for structural studies for the Raman experiment combined with the computations, we chose methacrylamide (A), piracetam (B), and 2-thiobarbituric acid (C) as model molecules representing typical organic systems forming polymorphic crystals (Figure 1). The differences

between their polymorphs range from a subtle change in the crystal packing (piracetam) over conformational (methacrylamide) and tautomeric (2-thiobarbituric acid) variations. Within DFT, we model Raman spectra of isolated molecules as well as take into account the crystal environment of model systems. A cluster crystal model and a periodic-boundary condition plane-wave computation are employed.

The industrially important compound methacrylamide is, for example, a key intermediate in the acetonecyanohydrin process employed in manufacturing methyl methacrylate.³ Of the two

Table 1. Overview of Studied Compounds and Their Crystal Structure

Compound	Form 1	Crystal ^a <i>a b c</i> (Å) <i>α β γ</i> (deg.)	Form 2	Crystal ^a <i>a b c</i> (Å) <i>α β γ</i> (deg.)	
methacrylamide Ref. ³		WANSAG07 9.365 6.086 9.743 90.00 115.30 90.00		WANSAG01 5.934 10.242 16.436 90.00 90.00 90.00	A
Piracetam		6.403 6.618 8.556 79.85 102.39 91.09		6.525 6.440 16.463 90.00 92.19 90.00	B
		RISMEN01 Ref. ²²			
		PABNAJ 9.874 8.776 7.066 90.00 109.30 90.00		THBARB01 9.523 7.703 8.002 90.00 105.68 90.00	C
				2-thiobarbituric acid Ref. ²⁶	

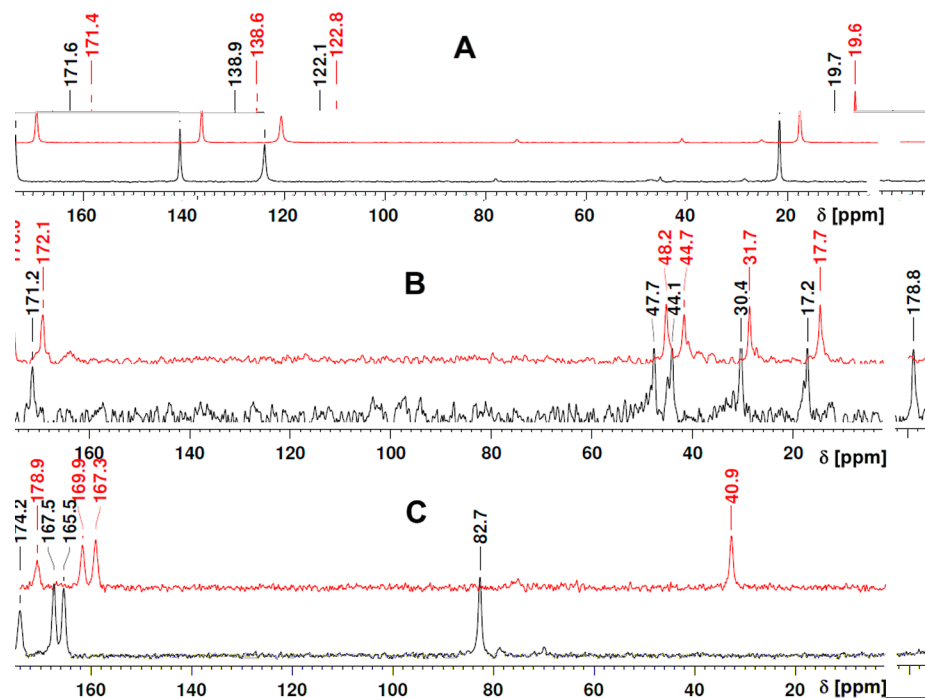
^aCambridge Structural Database ID and unit cell parameters.

Figure 2. ¹³C solid-state NMR spectra of polymorphic crystals. From top to bottom: **A1** vs **A2**, **B1** vs **B2**, and **C1** vs **C2**. For clarity, the forms **A1**, **B1**, and **C1** are plotted in red and offset by ~4 ppm; in **A**, the three low-intensity signals in the 20–80 ppm region correspond to spinning side bands of the sp² carbon atoms.

Powdered sulfur was used as a reference sample to check the wavenumber scale. A ChiralRAMAN-2X spectrometer provided a stronger signal, whereas the NIR-excited measurement reduced the fluorescence and provided a wider range of frequencies (–300 to 4500 cm^{–1}). The NIR Raman spectra are shown by default.

Raman and NMR Spectra Calculations. The atomic coordinates of the polymorphs of methacrylamide, piracetam, and 2-thiobarbituric acid were derived from the Cambridge Crystallographic Database³² (see Table 1 for the reference codes). The shielding values of the infinite crystals, harmonic force fields, and Raman intensities were calculated by using the CASTEP program.³³ The calculations were based on X-ray structures with positions of all atoms optimized by energy

minimization; the experimental lattice parameters were kept fixed. The generalized gradient approximation (GGA) functional of Perdew, Burke, and Ernzerhof (PBE)³⁴ and norm-conserving pseudopotentials were employed. Harmonic force field and Raman intensities within the periodic boundary conditions³⁵ were calculated at the same level as for the optimization. To verify reliability of the results, two combinations of the plane-wave cutoff energy and Monkhorst–Pack³⁶ grid spacing were applied (600 eV and 0.08 Å^{–1} and 900 eV and 0.05 Å^{–1}; the latter setup providing better results on average is presented by default). With the optimized geometries, NMR shielding was calculated using the gauge-including projector-augmented wave approach (GIPAW)³⁷ and the “on the fly” pseudopotentials at 550 eV cutoff.³⁸

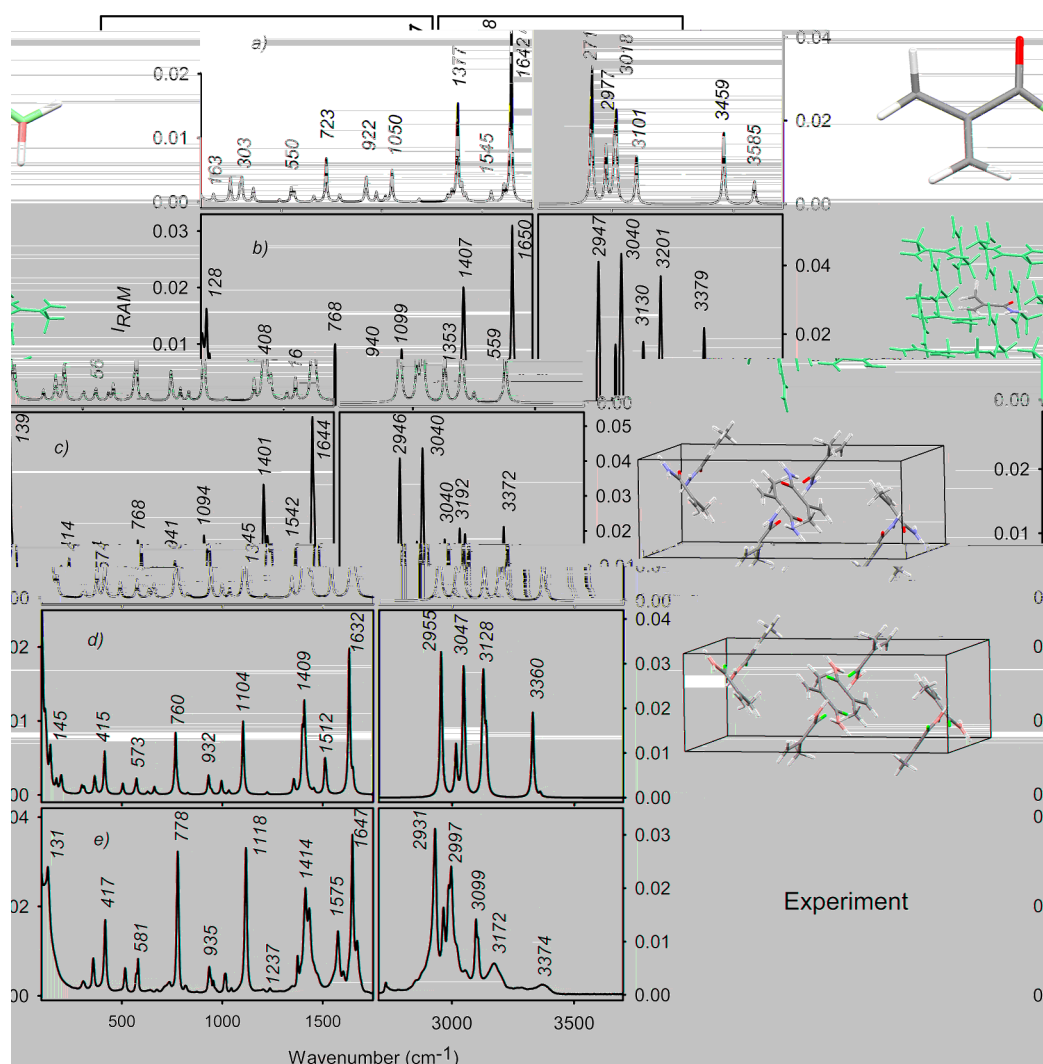


Figure 3. Raman spectra of methacrylamide, **A2**, computed for (a) single molecule and (b) a cluster. The (0,0,0) mode signals of the periodic elementary cell are in the (c) and (d) panels, while (e) is the experimental spectrum. Spectra a–c were obtained at the B3PW91/6-311++G**/6-31G/CPCM level and α -scaled by a factor of 0.96; (d) was obtained by the plane-wave simulation with the PBE functional.

As an alternative to the CASTEP “plane-wave” (PW) approach described above, we computed the Raman spectra with a cluster model and Gaussian atomic orbitals. First, the crystal cell obtained for each simulated system from the database was propagated to a “ $3 \times 3 \times 3$ ” packing geometry, replicating elementary cell directions. Then clusters of a molecule chosen in the center and neighboring molecules closer than 4 Å were created with our own software. Finally, the geometries of the clusters were optimized in normal mode vibrational coordinates^{39,40} with ω_{\max} ⁴¹ of 300 cm^{−1}. Note that such constrained optimization leaves the crystal geometry virtually unchanged, whereas the vibrational coordinates relevant to Raman spectrum (frequencies typically greater than ω_{\max}) can be relaxed.

The force field and polarizability derivatives of the clusters were then calculated by the Gaussian⁴² program and transferred^{43,44} back to the crystal cell. The BPW91⁴⁵ functional with the 6-31G and 6-31G** basis sets and the B3PW91^{46,47} functional with the 6-311++G** and 6-31G basis sets for the central and neighboring molecules, respectively, were used. The reduction of the basis set was necessary to obtain results in a reasonable computational time. Supposedly, however, the effect

of this approximation on the precision is limited as the diagonal force constants most important for the vibrational frequencies⁴⁸ were obtained from the central molecule with the larger basis set. The results were quite similar given the differences between the polymorphic forms; only the B3PW91/6-311++G**/6-31G calculations are shown, with the surrounding crystal environment simulated by placing the clusters in the CPCM model solvent⁴⁹ with relative electric permittivity $\epsilon_r = 78$. We used the water permittivity as reported earlier⁵⁰ to approximately mimic the dielectric properties of polar organic crystals. While the CPCM correction provided slightly better results than vacuum computations, we verified that the simulated spectra were fairly independent of the variation of ϵ_r .

From the plane wave model and cluster force fields, zero (0, 0, 0) crystal phonon mode vibrational frequencies were calculated. Involvement of phonon modes with nonzero wave vectors had a negligible effect on the simulated intensities. Theoretical spectra were simulated with the Lorentzian bands, and the full width at half-maximum (Δ) was set 10 cm^{−1}, while applying the Boltzmann temperature correction. The spectrum at frequency ω was obtained from the computed backscattering Raman intensities (I_{180}) of each mode i with the harmonic

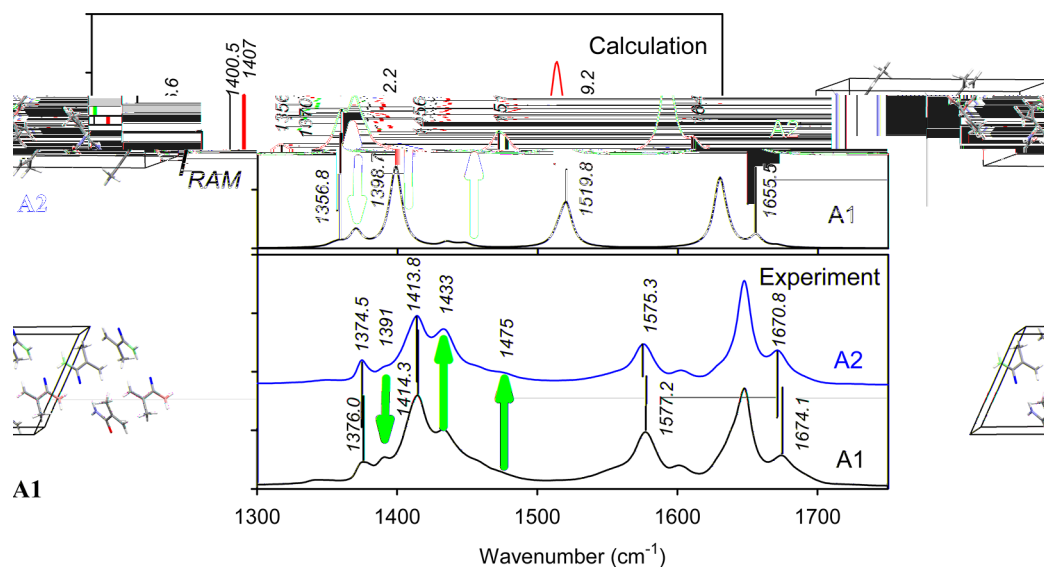


Figure 4. Calculated (top, plane wave) and experimental (bottom, NIR) Raman spectra of the two methacrylamide crystal forms, within 1300–1750 cm^{-1} . Main intensity changes are indicated by the blue arrows; selected peak maxima are indicated.

vibrational frequency ω_i as $S(\omega) = \omega_i^{-1} \{1 - \exp[-\omega_i/(kT)]\}^{-1} \{4[(\omega - \omega_i)/\Delta]^2 + 1\}^{-1} I_{180}$, where k is the Boltzmann constant and T is the temperature.

RESULTS

NMR Analysis. The NMR results were not the focus of the present study, as the detection of polymorphic forms by this technique has been previously described for a number of compounds.^{5,26,51} In Figure 2, ^{13}C solid-state NMR spectra of polymorphic forms of methacrylamide (A1, A2), piracetam (B1, B2), and 2-thiobarbituric acid (C1, C2) are plotted. It can be clearly seen that the crystal packing induces specific shielding; i.e., the samples used in the Raman measurement correspond to the required forms.

Curiously, only nonpure preparations of methacrylamide batches, i.e., those also containing one or the other form, have been described so far.³ As it is apparent from the NMR spectra (Figure 2), we did obtain pure forms of this compound. However, when sample A2 (prepared from water solution) was not completely dried before the CP-MAS experiment, it slowly transformed to A1. The process could be monitored in a series of successive CP-MAS spectra, in which the A2 signals were decreasing while the A1 ones were increasing. The A2 to A1 transformation may have been facilitated by the combined effect of residual solvent and higher pressure in the MAS rotor spinning at 12 kHz because it was not observed when the sample was dry or wet and stored without spinning.

The calculations reproduce the experimental differences in chemical shifts of the polymorphic forms quite well. Except for one atom, all predicted signs agree with the experiment, with a small average error of 1.5 ppm (δ , see Table S1). These results are in accord with our earlier study, where the solid state NMR spectroscopy was found to be very suitable for identification of the polymorphic forms and the crystal packing.⁵¹ The crystal packing is reflected in the chemical shift in two ways; it directly affects the electronic shielding by neighboring molecules and the geometry or conformational changes due to the packing itself.^{52,53} Either of these contributions can be estimated by the comparison shifts calculated for an isolated molecule (while employing either X-ray data or optimized geometry; see second

and third column in Table S1). However, as expected, the full periodic boundary computation (fourth column in Table S1) is needed to reach the best agreement with the experiment.

Theoretical Models Adopted for Raman Spectra. To understand the Raman spectral pattern, we adopted various models for its simulation. This is exemplified by the spectra of the A2 form plotted in Figure 3. The single-molecule computation performed at the B3PW91/6-31++G**/CPCM level (panel a in Figure 3) is compared to the spectrum of the cluster (b). In addition, the elementary cell signal was obtained from (b) by the CCT transfer⁴⁴ (c) and as the plane-wave PBE result (d). The experiment is plotted in panel e. The B3PW91 frequencies were scaled by a factor of 0.96 for an easier comparison.

The effect of the packing interactions is clearly manifested in spectra shown in Figure 3. The isolated molecule (a) provides the basic spectral pattern; however, it deviates in some features from the experiment (e). For example, there is no signal (except for the weak band of methyl rotation at 163 cm^{-1}) at the lowest wavenumbers, unlike in the experiment with a strong peak at 131 cm^{-1} ; the experimental band at 1575 cm^{-1} does not have a clear counterpart in the simulation, and the simulated bands at 3459 and 3585 cm^{-1} (in- and out-of-phase NH stretching, respectively) are too high.

The cluster model (b) provides a more realistic spectrum. In particular, the lowest wavenumber ($\sim 100\text{--}600 \text{ cm}^{-1}$) signal rises and is better structured than on (a), which reflects the crystal packing forces. These modes are to a large extent composed of delocalized translations/rotations of various molecular parts. Also, the NH out-of-phase stretching frequency dramatically falls to 3379 cm^{-1} , and the in-phase mode (3201 cm^{-1} in (b)) is even below the CH_2 group stretching. This corresponds to the uneven length of the $\text{NH}\cdots\text{O}$ hydrogen bonds in the crystal, 2.029 and 2.093 \AA ,³ contributing to the splitting of the NH stretching modes. It is also interesting to note that the PCM approximation of the bulk crystal adopted for the single-molecule spectrum a does not adequately represent the NH stretching frequency affected by the hydrogen bonding. Such inability of the polarizable continuum solvent models to fully describe the directional and

partially covalent hydrogen bonds has been well documented elsewhere.^{54–60}

Finally, spectra c and d obtained from the periodic elementary cell and the (0, 0, 0) phonon mode are the most realistic ones. The cluster-based model (c) provides a more realistic hydrogen-stretching pattern, in particular the 3192 cm^{-1} signal observable at 3172 cm^{-1} , and intensities above 1200 and below 200 cm^{-1} . On the other hand, some features, mostly within 200–1200 cm^{-1} , are better reproduced by the plane-wave calculation (d).

A visualization of the normal mode displacement reveals an interesting shift of the amide I ($\text{C}=\text{O}$ stretching) mode, in the single-molecule (a) hidden at the signal around 1642 cm^{-1} . This vibration heavily mixes with the in-phase NH bending and shifts downward in the crystal, to 1542 cm^{-1} for the cluster model c, experimentally at 1575 cm^{-1} . Note that the plane-wave approach can take into account the longer-scale electron conjugation and periodicity of the crystal structure, whereas the cluster model comprises interactions of the neighboring molecules only. On the other hand, the cluster approach enables one to use a more advanced functional (B3PW91, containing the Hartree–Fock exchange) and the more economical Gaussian basis set.

A1 and A2 Polymorphs. The differences between the individual polymorph spectra of methacrylamide (A1 vs A2, calculation vs experiment) are documented in Figure 4 showing the 1300–1750 cm^{-1} interval where the most significant spectral changes occurred. As it can be seen, individual polymorphs of this molecule differ in minor shape changes of the Raman bands.

The relative intensity and frequency changes between individual peaks in A1 and A2 spectra can easily be inspected visually (Figure 4). Experimentally, for example, the intensity at 1374.5 cm^{-1} of A2 partially moves to 1391 cm^{-1} for A1. Corresponding calculated peaks at 1356.6 and 1370 cm^{-1} reveal that this is caused by changes in mode coupling, rather than by shifts of the vibrational frequencies themselves. In particular, the CH_3 umbrella CH bending vibrations (experimentally $\sim 1376 \text{ cm}^{-1}$) couple differently with the other modes (NH_2 , CH_2 bending, C–C stretching), providing thus the intensity boost at 1370 cm^{-1} in A1.

Similarly, another strong signal for A2, experimentally at 1433 cm^{-1} , calculated at 1407 cm^{-1} , originates in CH scissoring modes coupled with other CH bending and C–C stretching. A minor band of A2 at 1475 cm^{-1} is caused primarily by CH_3 scissoring vibrations. The calculated band at 1512.2 cm^{-1} in A2 shifts to 1519.8 cm^{-1} in A1, as in experiment, although the observed change is smaller and the absolute frequency higher, at $\sim 1576 \text{ cm}^{-1}$. Because this frequency is underestimated in the cluster model as well (e.g., at 1542 cm^{-1} , spectrum c, Figure 3), the lack of anharmonic corrections in the model is the most likely scenario. Presently, we are not aware of any other method providing reliable anharmonic corrections for systems of this size.

It is important to understand that the main differences in the polymorphic spectra have in this case their origin in the crystal packing. The cis and trans conformations of individual methacrylamide molecules provide different spectra (cf. Figure S1) but do not explain the crystal features (Figure 3) or the polymorphic differences (Figure 4). Interestingly, the A1 and A2 crystal Raman spectra (see Figure S2 for a comparison in the entire range of frequencies) resemble more each other than those of the isolated cis and trans conformers (Figure S1). In

other words, crystal packing appears to smear the differences in the spectra of individual isomers.

Polymorphs B1 and B2. Piracetam behaves somewhat differently than methacrylamide. The B1 and B2 polymorphic forms are composed of very similar rotamers. The conformation in which the amide group is approximately perpendicular to the nearly planar five-membered ring is also conserved. The differences in the Raman spectra primarily arise from the different crystal packing, with the *P*-1 symmetry in B1 and *P*21/*n* in B2. Even then, the packing is quite similar,²² with a piracetam dimer being the basic unit held together by a dispersion attraction of the five-membered rings, and by hydrogen bonds between the NH_2 and exocyclic carbonyl groups. In B1, the dimer hydrogen bonds are slightly shorter (1.953 Å), and the ring is slightly more puckered than in B2 (cf. the N–C_O–C–C angle of 7°, Figure 5).

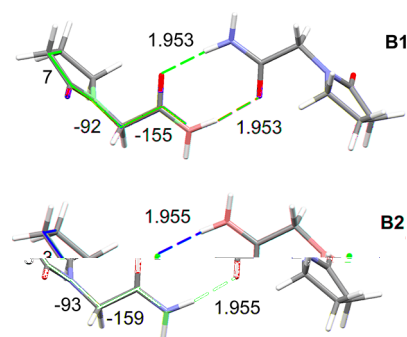


Figure 5. Piracetam dimer structure in two polymorphic crystal forms (distances in Å, torsional angles in deg).

The great degree of similarity between B1 and B2 causes only minor changes in the Raman spectra. The small effect of the packing on the spectra in an organic crystal is in agreement e.g. with a recent study⁶¹ about vibronic effects and solid state circular dichroism. However, as it can be seen in Figure 6 where the experiment from the 1064 nm excitation is compared to the plane-wave calculation, the differences exhibited as fine frequency and intensity changes occur within the entire range of frequencies and are reasonably matched by the computation.

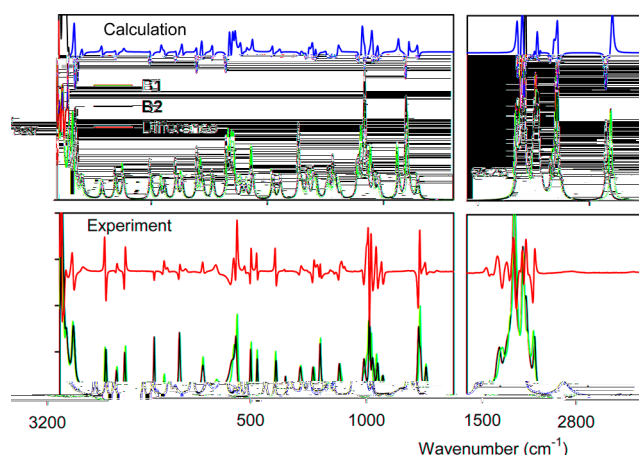


Figure 6. Calculated (top) and experimental (bottom) Raman spectra of the piracetam polymorphs B1 and B2. The intensity scale is arbitrary, but consistent in calculation and experiment; the intensities in the upper right panel are scaled down by a factor of 0.25.

The experimental spectrum obtained with the 532 nm laser is quite similar, and its comparison with a computed spectrum is shown in Figure S3. The correspondence between the simulation and the experiment is less clear in the hydrogen stretching region (2800–3400 cm^{-1} , Figure 6), most likely due to anharmonic forces⁶² that are difficult to include in the computation.⁶³ However, the theory provides correct signs of the intensity shifts of most bends including the most important intensity features of the difference spectrum plotted in Figure 6 in blue.

Alternatively, one can inspect the frequency change of individual vibrational bands for the two polymorphic forms. This analysis is more laborious than visual comparison of intensities as the corresponding peaks need to be identified. Nevertheless, as shown in Figure 7 where 10 vibrational bands

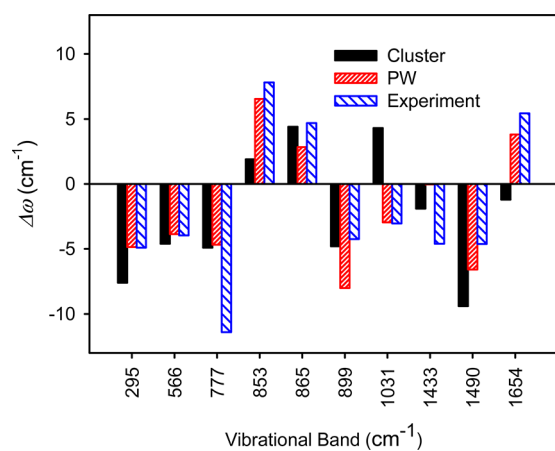


Figure 7. Ten largest frequency differences in the Raman bands between piracetam polymorphs, $\Delta\omega = \omega(\text{B1}) - \omega(\text{B2})$, calculated by the cluster and plane-wave method, and measured experimentally.

with the largest changes were selected, the frequency changes can also be quite reliably reproduced by the calculations. The plane-wave method appears to be more reliable than the cluster model; the latter one even yielded a frequency difference for the 1031 cm^{-1} Raman band with a wrong sign. Overall, however, the main trends are reproduced well. The large differences between the computation and experimental changes for 777 and 1433 cm^{-1} bands are at least partially explicable by an interference of close vibrations, indistinguishable at the currently available experimental resolution. On average, the changes computed by the PW method match the experiment with an error of only about 2 cm^{-1} and correlation coefficient of 0.739; the cluster results are noticeably worse (Figure S4).

The higher frequency (>2000 cm^{-1}) modes were not included in the statistics as they are difficult to assign and prone to anharmonic perturbations.^{62,64} Quite often, modes involving large hydrogen atom movements provide the largest frequency differences. These include the backbone torsion and CH_2 group rotation (experimentally at 295 cm^{-1}), NH_2 bending (853 cm^{-1}), torsion (865 cm^{-1}), or CH_2 scissor modes (1433 and 1490 cm^{-1}). The modes involving the amide oxygen (out-of-plane deviation at 566 cm^{-1} and $\text{C}=\text{O}$ stretching at 1606 cm^{-1}) also provide large frequency differences of about 5 cm^{-1} (Figure 7).

On piracetam, we can also demonstrate the effect of the energy cutoff and grid size on the computed Raman spectra (Figure S5). Both computational setups provided a reasonable

spectral shape, and for some bands the cruder model (500 eV, 0.08 Å) gave a better agreement with the experiment than the finer one (900 eV, 0.05 Å). However, the finer setup clearly performed overall better in terms of frequencies and relative peak intensities. The differences between the two polymorphic forms were significantly overestimated by the cruder model. Higher computational precision is thus required to capture the tiny differences in Raman spectra, as caused by crystal packing.

2-Thiobarbituric Acid Polymorphs C1 and C2. This compound exhibits yet another behavior than the previous two systems, with the greatest differences among the Raman spectra of its polymorphs. The simulated (plane-wave) and NIR Raman experimental spectra are plotted in Figure 8. In the hydrogen stretching region ($\sim 2800\text{--}3300$ cm^{-1}), for example, the C1 form has only one distinct peak in the experimental spectrum (3104 cm^{-1}), whereas C2 has three. This observation corresponds to the more extensive hydrogen bond network only compatible with the enol form C1 (cf. Table 1).²⁶ Computation yields more peaks in this region, but we can suppose that the NH stretching signals (3110, 3126, and 3222 cm^{-1} in Figure 8) are manifested as a broad background only in the experiment, due to the strong anharmonic effects and polarity of the hydrogen bond, similarly as for the OH stretching.

The plane-wave computation provided an unreasonable value of the OH stretching frequency (~ 2000 cm^{-1} , not shown), most probably due to the inaccuracy of the PBE functional unable to describe the very short hydrogen bond and a rather long OH bond observed in the crystal. The $\text{O}\cdots\text{H}$ and $\text{O}\text{--H}$ distances were determined as 1.44 and 1.097 Å, respectively.²⁶ Indeed, the OH vibration can be better reproduced with the cluster model where the B3PW91 functional can be used and where the signal at 2000 cm^{-1} disappears. However, this does not improve the overall agreement with the experiment (cluster computation, Figure S6). As expected, the single-molecule spectra, also plotted in Figure S6, are not realistic either. Most probably, the weak experimental signals of the OH and NH stretching bands are caused by anharmonic interactions and consequent inhomogeneous band broadening; the experimental band at 3104 cm^{-1} can then be assigned to C–H stretching.

In the experimental Raman spectrum of C2, three strong bands appear in the high-frequency region (Figure 8). The peaks at 2874 and 2979 cm^{-1} are reproduced by the calculation (2886 and 3036 cm^{-1}) as C–H stretching bands. Interestingly, the rather unusual low frequency of the experimental 2874 cm^{-1} band seems to be caused by a weak hydrogen bond involving an aliphatic hydrogen and keto group oxygen. The third experimental band at the highest frequency (3097 cm^{-1}) is reproduced as a split 3108/3131 cm^{-1} signal, which unmasks yet another loophole in the theory regarding the polar hydrogen bonding.

The spectra of the C1 and C2 forms are even more complex in the lower-frequency region (<1800 cm^{-1} , Figure 8), and the theory can faithfully reproduce only some experimental features. It should be also noted that the experimental spectrum C1 may contain incompletely subtracted contributions from C2. However, by a careful comparison, a reliable assignment of most peaks is possible. Only the C2 form provides the $\text{C}=\text{O}$ stretching (“amide I”) peak at 1717 cm^{-1} in the experiment, reproduced at 1657 cm^{-1} by the model. In C1, this mode is mixed with $\text{C}=\text{C}$ stretching, providing only a weak signal as reproduced by the calculation. The amide II mode (largely N–C stretching) shifts from the experimental 1553 cm^{-1} peak in

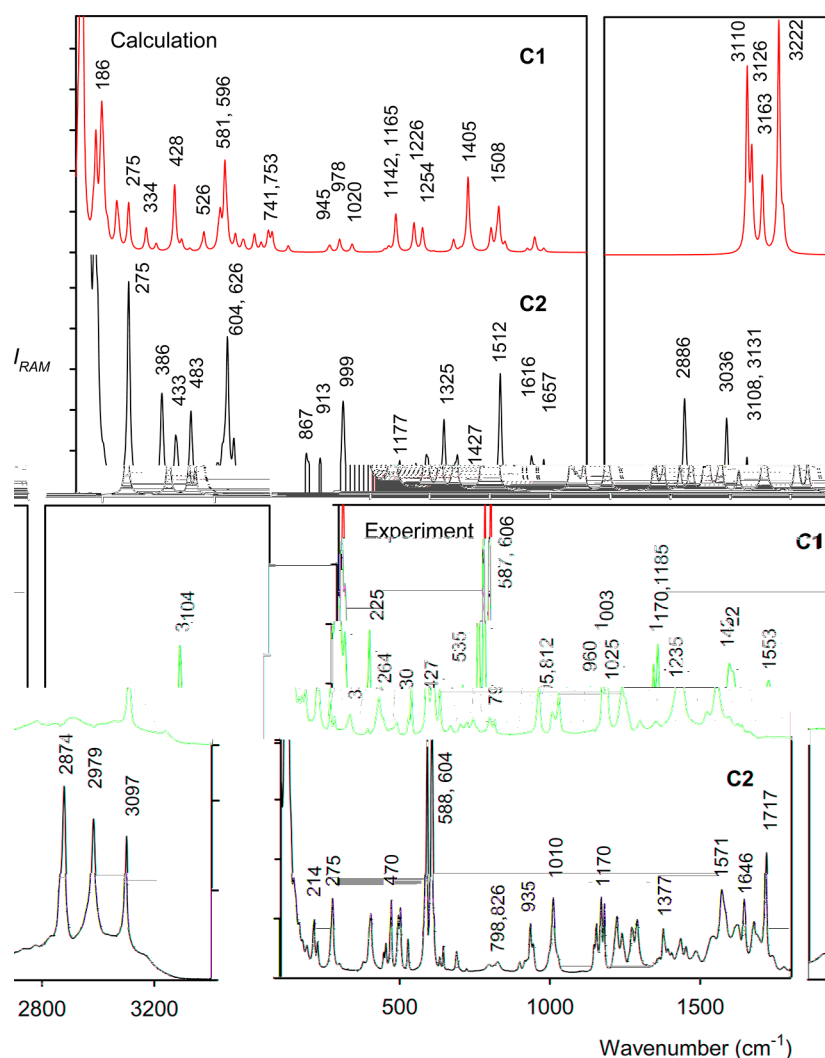


Figure 8. 2-Thiobarbituric acid: calculated (plane-wave) and NIR experimental Raman spectra of the two polymorphic forms C1 and C2.

C1 to 1571 cm^{-1} in C2, similarly as in theory ($1508 \rightarrow 1512 \text{ cm}^{-1}$). A ring deformation in C1 gives a strong signal both in the theoretical (1405 cm^{-1}) and observed (1422 cm^{-1}) spectrum, similarly as for the CH_2 scissoring mode in C2 (exptl 1377 cm^{-1} , calcd 1325 cm^{-1}). The experimental $\text{C}=\text{S}$ stretching band moves down from 1025 cm^{-1} (C1) to 1010 cm^{-1} (C2), as does the theoretical one ($1020 \rightarrow 999 \text{ cm}^{-1}$). A visual inspection of the normal modes reveals that $\text{C}=\text{S}$ stretching is also mixed with $\text{C}=\text{N}$ stretching, contributing to the signal around 1170 cm^{-1} .

A rather specific signal, clearly stronger in the C2 form, is due to out-of-plane motions, such as NH bending; it is experimentally observed at 798–935 cm^{-1} and calculated at 867–913 cm^{-1} . The strongest experimental intensities, detected at 587–606 cm^{-1} , are underestimated by the computation. They originate in the out-of-plane $\text{C}=\text{O}$, $\text{C}=\text{S}$, and $\text{C}-\text{H}$ group motions, which are notoriously difficult to describe within the harmonic approximation.^{57,65} Finally, the lowest-wavenumber region is also rich in information, involving, for example, the 526/535 (calcd/exptl) cm^{-1} or the 428/427 cm^{-1} ring deformation band characteristic for C1 and a very stable $\text{C}=\text{S}$ bending frequency (experimentally at 264/275 cm^{-1} for C1/C2).

Although the polymorphic differences can be reliably reproduced by our models, an accuracy improvement is certainly still needed. It is very likely that the accuracy of the GGA force field and Raman intensities obtained within the PW computations represent the limiting factor; the cluster approach is more flexible in the basis set and functional choice but limited in the physical model. The absolute Raman intensities in particular are extremely sensitive to the basis set variations.⁶⁶ For the C1/C2 polymorphic forms, a correction for anharmonic forces can potentially improve the hydrogen-stretching region (2800–3200 cm^{-1}). However, this is currently impossible for a system of this size. Additionally, larger deviations between the simulations and the experiment are also encountered in the lower-frequency region. Although this region is presumably well described at the harmonic level, frequency shifts of several cm^{-1} caused by anharmonic forces cannot be excluded. Future improvements of the method are thus dependent on the efficiency of implementing more precise electronic and vibrational quantum chemical methods.

Other structural information might also be hidden in the lattice modes, not analyzed in the present study. Our spectrometers do not enable measurement below $\sim 100 \text{ cm}^{-1}$. These vibrations are difficult to analyze because of the large background signal and a limited precision of calculated force

fields. Another important practical issue in the Raman spectra interpretation is the use of coordinates determined by X-ray diffraction. If one wants to replace X-ray spectroscopy, a pure a priori generation could be considered in the future for the initial coordinates as well. Currently, we propose the Raman technique as a convenient complementary way of examining the polymorphic forms in analytical practice.

■ CONCLUSIONS

We succeeded in preparing model polymorphic crystal forms of three model compounds including those of practical importance and characterized them by NMR and Raman spectroscopy. Pure polymorphs of methacrylamide were prepared, which has not been reported so far.

The NMR data confirmed sample purity and good performance of the technique in polymorphic discrimination. Raman spectroscopy proved to be an equally viable technique, as the spectra of different polymorphs exhibited distinct features that could be reliably reproduced by the density functional computations. Compared to green (532 nm) laser, excitation by a near-infrared one was somewhat more suitable as it suppressed sample fluorescence. The spectral shapes were similar in both experiments.

In spite of minor inconsistencies, the plane-wave approach, inherently comprising the crystal symmetry and periodicity, made it possible to reliably simulate spectral frequencies and intensities. Occasionally, the cluster-based computations were more advantageous as they could be combined with more theoretical approaches, in particular with different functionals. The studied examples represent a wide array of interpolymorphic differences manifested in the Raman spectra, from an almost pure crystal packing influence (piracetam) to profound changes in molecular structures (methacrylamide, 2-thiobarbituric acid). The computational models could successfully handle all cases, and we aim to further improve them so that even more complex systems can be reliably examined in the future. In any case, we demonstrated that Raman spectroscopy combined with computational modeling can significantly enhance the structural analysis of organic compounds' polymorphic forms.

■ ASSOCIATED CONTENT

📄 Supporting Information

Calculated and experimental chemical shifts, additional computational and experimental details. This material is available free of charge via the Internet at <http://pubs.acs.org>.

■ AUTHOR INFORMATION

Corresponding Author

*E-mail: bour@uochb.cas.cz (P.B.).

Notes

The authors declare no competing financial interest.

■ ACKNOWLEDGMENTS

The work was supported by the Academy of Sciences (M200551205), Czech Science Foundation (P208/11/0105 and 13-24880S), and Ministry of Education (LH11033). We thank Dr. Císařová for X-ray crystal characterization and Dr. Pelc for valuable comments.

■ REFERENCES

- (1) Bernstein, E. R. Polymorphism - a Perspective. *Cryst. Growth Des.* **2011**, *11*, 632–650.
- (2) Grant, D. J. W. Theory and Origin of Polymorphism. In *Polymorphism in Pharmaceutical Solids*; Brittain, H. G., Ed.; Marcel Dekker, Inc.: New York, 1999.
- (3) Guo, C. Y.; Hickey, M. B.; Guggenheim, E. R.; Enkelmann, V.; Foxman, B. M. Conformational Polymorphism of Methacrylamide. *Chem. Commun.* **2005**, *17*, 2220–2222.
- (4) Anderson, K. M.; Steed, J. W. Comment on “On the Presence of Multiple Molecules in the Crystal Asymmetric Unit ($Z' > 1$)” by Gautam R. Desiraju. *CrystEngComm* **2007**, *9*, 328–330.
- (5) Harris, R. K. NMR Studies of Organic Polymorphs & Solvates. *Analyst* **2006**, *131*, 351–373.
- (6) Saurabh, G.; Kaushal, C. Pharmaceutical Solid Polymorphism in Abbreviated New Drug Application (ANDA) - a Regulatory Perspective. *J. Chem. Pharm. Res.* **2011**, *3*, 6–17.
- (7) Datta, S.; Grant, D. J. W. Crystal Structures of Drugs: Advances in Determination, Prediction and Engineering. *Nat. Rev. Drug Discovery* **2004**, *3*, 42–57.
- (8) Wu, V.; Rades, T.; Saville, D. J. Stability of Polymorphic Forms of Ranitidine Hydrochloride. *Pharmazie* **2000**, *55*, 508–512.
- (9) Seddon, K. R. Perspective - Pseudopolymorph: A Polemic. *Cryst. Growth Des.* **2004**, *4*, 1087–1087.
- (10) Anderson, K. M.; Probert, M. R.; Whiteley, C. N.; Rowland, A. M.; Goeta, A. E.; Steed, J. W. Designing Co-Crystals of Pharmaceutically Relevant Compounds That Crystallize with $Z' > 1$. *Cryst. Growth Des.* **2009**, *9*, 1082–1087.
- (11) Rummel, R. J. *Applied Factor Analysis*; Northwestern University Press: Evanston, 1970.
- (12) Aliev, A. E.; Mann, S. E.; Rahman, A. S.; McMillan, P. F.; Cora, F.; Iuga, D.; Hughes, C. E.; Harris, K. D. M. High-Resolution Solid-State ^2H NMR Spectroscopy of Polymorphs of Glycine. *J. Phys. Chem. A* **2011**, *115*, 12201–12211.
- (13) Langan, P.; Mason, S. A.; Myles, D.; Schoenborn, B. P. Structure and Characterization of Crystals of $\text{Alph2(C.)-89/F3R13.7.8(a)}$. *Chem. Commun.* **2011**, 12201–12211.

- (23) Bandoli, G.; Clemente, D. A.; Grassi, A.; Pappalardo, G. C. Molecular Determinants for Drug-Receptor Interactions. 1. Solid-State Structure and Conformation of the Novel Nootropic Agent 2-Pyrrolidone-N-Acetamide - X-Ray and Theoretical SCF-MO Studies. *Mol. Pharmacol.* **1981**, *20*, 558–564.
- (24) Louër, D.; Louër, M.; Dzyabchenko, V. A.; Agafonov, V.; Céolin, R. Structure of a Metastable Phase of Piracetam from X-Ray-Powder Diffraction Using Atom-Atom Potential Method. *Acta Crystallogr., Sect. B* **1995**, *51*, 182–187.
- (25) Bondock, S.; Tarhoni, A. E.; Fadda, A. A. *Phosphorus, Sulfur Silicon Relat. Elem.* **2007**, *182*, 1915–1936.
- (26) Chierotti, M. R.; Ferrero, L.; Garino, N.; Gobetto, R.; Pellegrino, L.; Braga, D.; Grepioni, F.; Maini, L. The Richest Collection of Tautomeric Polymorphs: The Case of 2-Thiobarbituric Acid. *Chem.—Eur. J.* **2010**, *16*, 4347–4358.
- (27) Calas, M. R.; Martinez, J. Determination de la Structure Cristalline de l'Acide Thiobarbiturique. *C. R. Acad. Sci., Ser. C* **1967**, *265*, 631–631.
- (28) Altomare, A.; Casciaro, G.; Giacovazzo, C.; Guagliardi, A.; Burla, M. C.; Polidori, G.; Camalli, M. SIR92 - a Program for Automatic Solution of Crystal Structures by Direct Methods. *J. Appl. Crystallogr.* **1994**, *27*, 435.
- (29) Sheldrick, G. M. A Short History of SHELX. *Acta Crystallogr., Sect. A* **2007**, *64*, 112–122.
- (30) Hug, W.; Hangartner, G. A Novel High-Throughput Raman Spectrometer for Polarization Difference Measurements. *J. Raman Spectrosc.* **1999**, *30*, 841–852.
- (31) Šebestík, J.; Bouř, P. Raman Optical Activity of Methyloxirane Gas and Liquid. *J. Phys. Chem. Lett.* **2011**, *2*, 498–502.
- (32) Allen, F. H. The Cambridge Structural Database: A Quarter of a Million Crystal Structures and Rising. *Acta Crystallogr., Sect. B* **2002**, *58*, 380–388.
- (33) Clark, S. J.; Segall, M. D.; Pickard, C. J.; Hasnip, P. J.; Probert, M. J.; Refson, K.; Payne, M. C. First Principles Methods Using CASTEP. *Z. Kristallogr.* **2005**, *220*, 567–570.
- (34) Perdew, J. P.; Burke, K.; Ernzerhof, M. Generalized Gradient Approximation Made Simple. *Phys. Rev. Lett.* **1996**, *77*, 3865–3868.
- (35) Refson, K.; Tulip, P. R.; Clark, S. J. Variational Density-Functional Perturbation Theory for Dielectrics and Lattice Dynamics. *Phys. Rev. B* **2006**, *73*, 155114.
- (36) Monkhorst, H. J.; Pack, J. D. Special Points for Brillouin-Zone Integrations. *Phys. Rev. B* **1976**, *13*, 5188–5192.
- (37) Pickard, C. J.; Mauri, F. All-Electron Magnetic Response with Pseudopotentials: NMR Chemical Shifts. *Phys. Rev. B* **2001**, *63*, 245101.
- (38) Yates, J. R.; Pickard, C. J.; Mauri, F. Calculation of NMR Chemical Shifts for Extended Systems Using Ultrasoft Pseudopotentials. *Phys. Rev. B* **2007**, *76*, 024401.
- (39) Bouř, P.; Keiderling, T. A. Partial Optimization of Molecular Geometry in Normal Coordinates and Use as a Tool for Simulation of Vibrational Spectra. *J. Chem. Phys.* **2002**, *117*, 4126–4132.
- (40) Bouř, P. Convergence Properties of the Normal Mode Optimization and Its Combination with Molecular Geometry Constraints. *Collect. Czech. Chem. Commun.* **2005**, *70*, 1315–1340.
- (41) Hudecová, J.; Hopmann, K. H.; Bouř, P. Correction of Vibrational Broadening in Molecular Dynamics Clusters with the Normal Mode Optimization Method. *J. Phys. Chem. B* **2012**, *116*, 336–342.
- (42) Frisch, M. J.; Trucks, G. W.; Schlegel, H. B.; Scuseria, G. E.; Robb, M. A.; Cheeseman, J. R.; Scalmani, G.; Barone, V.; Mennucci, B.; Petersson, G. A.; et al. *Gaussian 09, Revision B01*; Gaussian, Inc.: Wallingford, CT, 2009.
- (43) Bouř, P.; Sopková, J.; Bednářová, L.; Maloň, P.; Keiderling, T. A. Transfer of Molecular Property Tensors in Cartesian Coordinates: A New Algorithm for Simulation of Vibrational Spectra. *J. Comput. Chem.* **1997**, *18*, 646–659.
- (44) Yamamoto, S.; Li, X.; Ruud, K.; Bouř, P. Transferability of Various Molecular Property Tensors in Vibrational Spectroscopy. *J. Chem. Theory Comput.* **2012**, *8*, 977–985.
- (45) Becke, A. Density-Functional Exchange-Energy Approximation with Correct Asymptotic Behavior. *Phys. Rev. A* **1988**, *38*, 3098–3100.
- (46) Perdew, J. P.; Burke, K.; Wang, Y. Generalized Gradient Approximation for the Exchange-Correlation Hole of a Many-Electron System. *Phys. Rev. B* **1996**, *54*, 16533–16539.
- (47) Becke, A. D. Density-Functional Thermochemistry. III. The Role of Exact Exchange. *J. Chem. Phys.* **1993**, *98*, 5648–5652.
- (48) Bouř, P.; Andrushchenko, V.; Kabeláč, M.; Maharaj, V.; Wieser, H. Simulations of Structure and Vibrational Spectra of Deoxyoctanucleotides. *J. Phys. Chem. B* **2005**, *109*, 20579–20578.
- (49) Klamt, A. COSMO and COSMO-RS. In *The Encyclopedia of Computational Chemistry*; Schleyer, P. R., Allinger, N. L., Clark, T., Gasteiger, J., Kollman, P. A., Schaefer III, H. F., Schreiner, P. R., Eds.; John Wiley & Sons: Chichester, 1998; Vol. 1, pp 604–615.
- (50) Kapitán, J.; Baumruk, V.; Kopecký, V., Jr.; Pohl, R.; Bouř, P. Proline Zwitterion Dynamics in Solution, Glass and Crystalline State. *J. Am. Chem. Soc.* **2006**, *128*, 13451–13462.
- (51) Dračinský, M.; Buděšínský, M.; Warzajtis, B.; Rychlewska, U. Solution and Solid-State Effects on NMR Chemical Shifts in Sesquiterpene Lactones: NMR, X-Ray, and Theoretical Methods. *J. Phys. Chem. A* **2012**, *116*, 680–688.
- (52) Dračinský, M.; Bouř, P. Computational Analysis of Solvent Effects in NMR Spectroscopy. *J. Chem. Theory Comput.* **2010**, *6*, 288–299.
- (53) Uldry, A. C.; Griffin, J. M.; Yates, J. R.; Perez-Torralba, M.; Maria, M. D. S.; Webber, A. L.; Beaumont, M. L. L.; Samoson, A.; Claramunt, R. M.; Pickard, C. J.; Brown, S. P. Quantifying Weak Hydrogen Bonding in Uracil and 4-Cyano-4'-Ethynylbiphenyl: A Combined Computational and Experimental Investigation of NMR Chemical Shifts in the Solid State. *J. Am. Chem. Soc.* **2008**, *130*, 945–954.
- (54) Ganim, Z.; Chung, H. S.; Smith, A. W.; Deflores, L. P.; Jones, K. C.; Tokmakoff, A.; Amide, I. Two-Dimensional Infrared Spectroscopy of Proteins. *Acc. Chem. Res.* **2008**, *41*, 432–441.
- (55) Lee, K. K.; Hahn, S.; Oh, K. I.; Choi, J. S.; Joo, C.; Lee, H.; Han, H.; Cho, M. Structure of N-Acetylproline Amide in Liquid Water: Experimentally Measured and Numerically Simulated Infrared and Vibrational Circular Dichroism Spectra. *J. Phys. Chem. B* **2006**, *110*, 18834–18843.
- (56) Choi, J. H.; Kim, J. S.; Cho, M.; Amide, I. Vibrational Circular Dichroism of Polypeptides: Generalized Fragmentation Approximation Method. *J. Chem. Phys.* **2005**, *122*, 174903.
- (57) Andrushchenko, V.; Matějka, P.; Anderson, D. T.; Kaminský, J.; Horníček, J.; Paulson, L. O.; Bouř, P. Solvent Dependence of the N-Methylacetamide Structure and Force Field. *J. Phys. Chem. A* **2009**, *113*, 9727–9736.
- (58) Bouř, P.; Michalík, D.; Kapitán, J. Empirical Solvent Correction for Multiple Amide Group Vibrational Modes. *J. Chem. Phys.* **2005**, *122*, 144501.
- (59) Bouř, P. On the Influence of the Water Electrostatic Field on the Amide Group Vibrational Frequencies. *J. Chem. Phys.* **2004**, *121*, 7545–7548.
- (60) Bouř, P.; Keiderling, T. A. Empirical Modeling of the Peptide Amide I Band IR Intensity in Water Solution. *J. Chem. Phys.* **2003**, *119*, 11253–11262.
- (61) Pescitelli, G.; Padula, D.; Santoro, F. Intermolecular Exciton Coupling and Vibronic Effects in Solid-State Circular Dichroism: A Case Study. *Phys. Chem. Chem. Phys.* **2013**, *15*, 795–802.
- (62) Daněček, P.; Bouř, P. Comparison of the Numerical Stability of Methods for Anharmonic Calculations of Vibrational Molecular Energies. *J. Chem. Phys.* **2009**, *131*, 084101.

(66) Zuber, G.; Hug, W. Rarefied Basis Sets for the Calculation of Optical Tensors. 1. The Importance of Gradients on Hydrogen Atoms for the Raman Scattering Tensor. *J. Phys. Chem. A* **2004**, *108*, 2108–2118.